

Reinforcement learning for online hyperparameter tuning in convex quadratic programming

Jeremy Bertoncini* Alberto De Marchi† Matthias Gerdt§ Simon Gottschalk§

Abstract

Quadratic programming is a workhorse of modern nonlinear optimization, control, and data science. Although regularized methods offer convergence guarantees under minimal assumptions on the problem data, they can exhibit the slow tail-convergence typical of first-order schemes, thus requiring many iterations to achieve high-accuracy solutions. Moreover, hyperparameter tuning significantly impacts on the solver performance but how to find an appropriate parameter configuration remains an elusive research question. To address these issues, we explore how data-driven approaches can accelerate the solution process. Aiming at high-accuracy solutions, we focus on a stabilized interior-point solver and carefully handle its two-loop flow and control parameters. We will show that reinforcement learning can make a significant contribution to facilitating the solver tuning and to speeding up the optimization process. Numerical experiments demonstrate that, after a lightweight training, the learned policy generalizes well to different problem classes with varying dimensions and to various solver configurations.

Keywords Quadratic programming, Reinforcement learning, Amortized optimization, Solver tuning, Acceleration strategies.

1 Introduction

Quadratic programming provides a fundamental optimization model with applications in finance, data analysis, robotics, process control, and operations research. A quadratic program (QP) with n variables, m equality constraints, and p inequality constraints can be written in the form

$$\underset{x \in \mathbb{R}^n}{\text{minimize}} \quad \frac{1}{2}x^\top Qx + q^\top x \quad \text{subject to} \quad Ax = b, \quad Gx \leq d \quad (1)$$

where $x \in \mathbb{R}^n$ is the optimization variable, $Q \in \mathbb{R}^{n \times n}$ is a symmetric positive semi-definite matrix that defines the quadratic cost, $q \in \mathbb{R}^n$ is the linear cost vector, matrix $A \in \mathbb{R}^{m \times n}$ with vector $b \in \mathbb{R}^m$ define the linear equality constraints, and matrix $G \in \mathbb{R}^{p \times n}$ with vector $d \in \mathbb{R}^p$ represent the linear inequality constraints. The nonnegative integers n , m and p denote the number of decision variables, equality and inequality constraints, respectively.

Methods for the numerical solution of QPs have been extensively studied. These differ in how they balance the number of iterations and the computational cost for each iteration. First-order methods, such as OSQP [37] based on ADMM [7], build upon simple steps but typically require many iterations, so several acceleration schemes have been proposed [18, 22, 2, 12]. In contrast, Newton-type methods such as interior point (IP) [8, 16, 15], active set [14] and semismooth Newton [26] usually need fewer, yet more demanding, iterations to reach accurate solutions. Recently, proximal techniques [29] and

*EMAIL jeremy.bertoncini@unibw.de, ORCID [0009-0003-6093-7532](https://orcid.org/0009-0003-6093-7532).

†EMAIL alberto.demarchi@unibw.de, ORCID [0000-0002-3545-6898](https://orcid.org/0000-0002-3545-6898).

‡EMAIL matthias.gerdt@unibw.de, ORCID [0000-0001-8674-5764](https://orcid.org/0000-0001-8674-5764).

§EMAIL simon.gottschalk@unibw.de, ORCID [0000-0003-4305-5290](https://orcid.org/0000-0003-4305-5290).

The authors are with the Department of Aerospace Engineering, Institute of Applied Mathematics and Scientific Computing, University of the Bundeswehr Munich, Werner-Heisenberg-Weg 39, 85577 Neubiberg, Germany.

This research is funded by dtcc.bw – Digitalization and Technology Research Center of the Bundeswehr [MissionLab, SeRANIS]. dtcc.bw is funded by the European Union – NextGenerationEU.

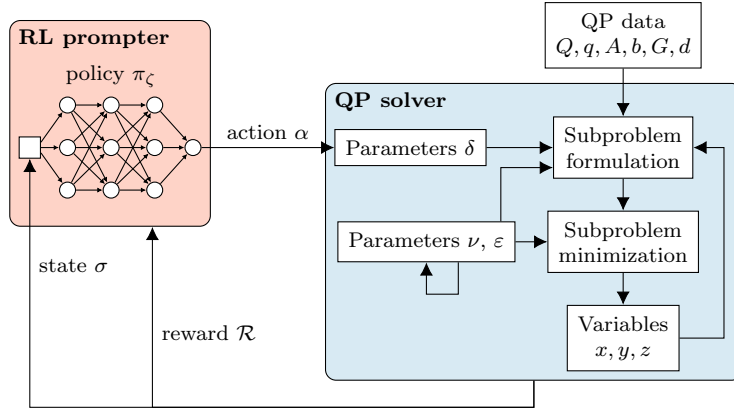


Figure 1: A QP solver is combined with a reinforcement learning (RL) agent that evaluates a policy to adapt the internal parameters of the QP solver. Based on its observation of the state of the environment, the RL action aims at improving the solver’s performance. The RL policy is parameterized by a small artificial neural network, the state σ summarizes the internal state of the QP solver (at the beginning of each inner loop), the action α affects the parameters δ of the solver, and the reward \mathcal{R} promotes faster convergence to a solution of the QP. Illustration inspired by [22, Fig. 1].

the augmented Lagrangian (AL) framework [31] have seen a resurgent interest due to their inherent regularization properties, resulting in the development of solvers such as QPDO [10], QPALM [21] and ProxQP [4]. On this vein, the integration of proximal regularization with the IP strategy led to IP-PMM [30], PS-IPM [9] and PIQP [36]. Thanks to proximal regularization, these solvers can cope with matrix Q merely positive semi-definite and with matrices A, G having linearly dependent rows.

Although convergence guarantees can be established under minimal requirements on the problem data and algorithmic parameters, there are often numerous hyperparameters that must be tuned to speed up convergence, and few clues on how to adjust them. Furthermore, in proximally regularized methods, the stepsize parameters not only affect the convergence rate but they also impact on the stability of linear algebra operations; cf. [9, §4]. Some theoretical works seek optimal values for the stepsize parameters, but they rely on solving auxiliary problems that are harder than the original QP itself [18, 19]. Another offline tuning approach is that of OPAL [3], which takes an algorithm as input and returns a recommendation on parameter values that maximize some user-defined performance metric. Alternatively, online heuristics introduce “feedback” by monitoring progress and adapting the parameters along the optimization process; see [6, §2], [37, §5.2], [21, §5.3] for some common instances.

After the seminal work [24] on “learning to optimize” for automated algorithm design, several researchers approached acceleration, warm-starting and hyperparameter tuning as machine learning tasks. A modern view on this computational approach is presented in the tutorial [1] on “amortized optimization” methods, which use learning to predict the solutions to problems by exploiting the shared structure between similar problem instances.

Despite the flexibility of learning-based methodologies, considerable attention was devoted to accelerating *first-order* optimization methods, driven by their scalability and applications in machine learning. Exemplarily, the architecture proposed in [33] consists of a neural network mapping from the QP problem data to warm-starts, learned across families of QPs. Dedicated to proximal methods for image processing, the tuning-free approach of [40] formulates the online hyperparameter selection as a sequential decision-making problem and implements a policy network for automated parameter search. Closer to our focus here is RLQP [22], which couples the OSQP solver with a reinforcement learning (RL) agent: by learning a policy to adapt the internal parameters of the ADMM algorithm, RLQP can outperform OSQP (with its fine-tuned heuristic update rules) on a variety of problems.

In contrast, the combination of learning techniques and *second-order*, or Newton-type, methods remains relatively unexplored. We investigate the coupling of a regularized IP solver for QPs with a policy for online hyperparameter tuning, parametrized with a simple neural network and learned by RL. Compared to the single-loop structure of OSQP, the architecture arising from an IP scheme can be represented with two nested loops, where each inner loop corresponds to the approximate solution of a subproblem

(by executing some iterations of Newton method); see Figure 1. While ubiquitous in second-order methods and with well established convergence theory, the two-loop structure does not fit the RL framework developed for RLQP, because of endogenous parameter sequences controlling the solution process (and affecting the MDP formalization). We aim to fill this gap by exploring a machine learning framework suitable for accelerating the tuning and solution process of QP solvers beyond first-order methods.

Contribution We formulate a RL framework to learn a policy for effective and reliable hyperparameter tuning, with the QP solver retaining provable convergence guarantees. The definitions of state, action and reward are intended (i) to yield a policy that is invariant to problem size, scaling and permutations, and (ii) to expose other internal parameters that drive the solver’s convergence.

Experimental results on random and benchmark QPs demonstrate that the learned policy performs well on previously unseen problem sizes, scales and classes, where tedious hand-tuning is usually needed. Moreover, these capabilities emerge after a lightweight training of a relatively small neural network, running on a standard laptop, compared to the prohibitive training for RLQP.

Outline Convex quadratic programming is introduced in Section 2 with a stabilized IP numerical scheme and a discussion on the challenges and opportunities of hyperparameter tuning. An overview of reinforcement learning is given in Section 3, with the tools needed to properly interact with the QP solver. Training procedures and numerical results for three evaluation settings are then presented in Section 4. We conclude with some final remarks in Section 5.

2 Solving convex QPs

In view of IP methods, the QP problem (1) can be equivalently formulated using an auxiliary variable $s \in \mathbb{R}^p$ as

$$\underset{x \in \mathbb{R}^n, s \in \mathbb{R}^p}{\text{minimize}} \quad \frac{1}{2}x^\top Qx + q^\top x \quad \text{subject to} \quad Ax = b, \quad Gx - d + s = 0, \quad s \geq 0. \quad (2)$$

It is a standard result that, for convex QPs, the following necessary conditions are also sufficient for optimality: there exists Lagrange multipliers $y \in \mathbb{R}^m$ and $z \in \mathbb{R}^p$ such that

$$0 = Qx + q + A^\top y + G^\top z, \quad 0 = \min\{s, z\}, \quad 0 = Ax - b, \quad \text{and} \quad 0 = Gx - d + s, \quad (3)$$

where the second equality coincides with the complementarity condition $0 \leq s \perp z \geq 0$. Therefore, a valid criterion for returning a triplet (x, y, z) as approximately optimal, with tolerance $\epsilon \geq 0$, is to check that the conditions

$$r_{\text{prim}}(x, y, z) := \left\| \begin{matrix} Ax - b \\ \min\{d - Gx, z\} \end{matrix} \right\|_\infty \leq \epsilon \quad \text{and} \quad r_{\text{dual}}(x, y, z) := \|Qx + q + A^\top y + G^\top z\|_\infty \leq \epsilon \quad (4)$$

are satisfied. The primal r_{prim} and dual r_{dual} residual functions indicate how far a triplet (x, y, z) is from being a primal-dual solution to (1), in view of (3). As such, these metrics will play a crucial role in monitoring and quantifying the performance of a solution process.

2.1 Regularized interior point schemes

Moving towards numerical schemes, we notice that, from an operator perspective, (3) is equivalent to a monotone inclusion. Adopting the (inexact) proximal point algorithm (PPA) [32, 27], different reformulations of (3) lead to different regularized schemes, whose subproblems correspond to the (approximate) evaluation of the proximal operator. This construction naturally gives rise to two-loop algorithms: the outer for PPA and the inner for the subproblem solution. Among others, QPDO [10] and PS-IPM [9] have been developed in this spirit, so that proximally regularized subproblems can be (efficiently and reliably) solved with Newton-type methods.

Here we outline a regularized IP scheme that, reminiscent of QPDO and PS-IPM, treats equality and inequality constraints respectively with primal-dual augmented Lagrangian and barrier strategies. For further regularization, a Tikhonov-like proximal term is included to handle also non-strictly convex QPs, as in [4, 5, 37].

Primal IP Beginning from the classical augmented Lagrangian function for (2), for any given primal-dual estimate $\theta = (\theta_x, \theta_y, \theta_z) \in \mathbb{R}^{n+m+p}$, regularization parameter $\delta = (\delta_x, \delta_y, \delta_z) \in \mathbb{R}_{++}^3$ and barrier parameter $\nu > 0$ (\mathbb{R}_{++} denotes the set of strictly positive real numbers), we define the merit function $\mathcal{L}_\delta(\cdot, \cdot; \theta, \nu) : \mathbb{R}^n \times \mathbb{R}_{++}^p \rightarrow \mathbb{R}$ as

$$\begin{aligned} \mathcal{L}_\delta(x, s; \theta, \nu) := & \frac{1}{2} x^\top Q x + q^\top x + \langle \theta_y, Ax - b \rangle + \langle \theta_z, Gx - d + s \rangle \\ & + \frac{\delta_x}{2} \|x - \theta_x\|^2 + \frac{1}{2\delta_y} \|Ax - b\|^2 + \frac{1}{2\delta_z} \|Gx - d + s\|^2 - \nu \sum_i \log s_i. \end{aligned} \quad (5)$$

As usual in barrier methods, the positivity constraint $s \geq 0$ in (2) is incorporated in a smooth way by replacing its indicator with a (logarithmic) barrier function: the smaller the barrier parameter ν , the better the approximation. Note that, for any fixed θ , δ and ν , $\mathcal{L}_\delta(\cdot, \cdot; \theta, \nu)$ is strictly convex under mere convexity of (1). Hence, it always admits a unique minimizer (x, s) that necessarily satisfies $s > 0$. Effectively, the minimization of $\mathcal{L}_\delta(\cdot, \cdot; \theta, \nu)$ constitutes a suitable subproblem for tackling (1), since its minimizer is closely related to the proximal point of an operator associated to (3); see [31, 9].

In practice, by minimizing $\mathcal{L}_{\delta^k}(\cdot, \cdot; \theta^k, \nu_k)$ one can obtain an improved primal estimate (x^k, s^k) and classical multiplier updates from AL methods yield a dual estimate (y^k, z^k) as

$$y^k \leftarrow \theta_y^k + \frac{Ax^k - b}{\delta_{y,k}} \quad \text{and} \quad z^k \leftarrow \theta_z^k + \frac{Gx^k - d + s^k}{\delta_{z,k}}. \quad (6)$$

After updating the incumbent estimate θ^{k+1} and the hyperparameters δ^{k+1} and ν_{k+1} , typically based on (x^k, s^k, y^k, z^k) , one moves on to the next subproblem.

Primal-dual IP A widespread technique is that of *primal-dual* interior point methods, where the subproblem is modified to involve both primal and dual variables, so that improved values for (y, z) are directly obtained from the inner minimization procedure. One way to generate a suitable subproblem for this task is to adopt the primal-dual augmented Lagrangian function, introduced by Gill and Robinson [17]. We define it as

$$\mathcal{M}_\delta(x, s, y, z; \theta, \nu) := \mathcal{L}_\delta(x, s; \theta, \nu) + \frac{1}{2\delta_y} \|Ax - b + \delta_y(\theta_y - y)\|^2 + \frac{1}{2\delta_z} \|Gx - d + s + \delta_z(\theta_z - z)\|^2 \quad (7)$$

where the additional terms guarantee that, when minimizing $\mathcal{M}_{\delta^k}(\cdot, \cdot, \cdot, \cdot; \theta^k, \nu_k)$ exactly, the optimal values for (y, z) coincide with the classical update (6) that would be performed within a purely primal scheme.

Algorithm 2.1: Regularized interior point method for convex QPs: primal-dual variant.

Data: primal-dual guess (x, y, z) , tolerance ϵ

```

1  $\theta^0 \leftarrow (x, y, z)$ 
2 for  $k = 0, 1, 2, \dots$  do
3   choose hyperparameters  $\delta^k, \nu_k, \epsilon_k$ 
4   define  $\mathcal{M}_k := (x, s, y, z) \mapsto \mathcal{M}_{\delta^k}(x, s, y, z; \theta^k, \nu_k)$ 
5   find  $(x^k, s^k, y^k, z^k)$  such that  $\|\nabla \mathcal{M}_k(x^k, s^k, y^k, z^k)\| \leq \epsilon_k$  and  $s^k > 0$ 
6   if  $r_{\text{prim}}(x^k, y^k, z^k) \leq \epsilon$  and  $r_{\text{dual}}(x^k, y^k, z^k) \leq \epsilon$  then return  $(x^k, y^k, z^k)$ 
7   set  $\theta^{k+1} \leftarrow (x^k, y^k, z^k)$ 
```

The resulting primal-dual scheme is outlined in Algorithm 2.1, where Step 5 poses the most computational requirements and will be discussed in the following Section 2.2. The termination conditions (4) are checked at Step 6, before updating the incumbent primal-dual estimate θ^{k+1} at Step 7. Of all steps, the choice of hyperparameters δ^k , ν_k and ϵ_k at Step 3 remains the most elusive, with minimal guidelines dictated by the theory. Their tuning and influence on the solution process are discussed in Section 2.3 below.

Convergence of Algorithm 2.1 is guaranteed whenever the regularization parameters δ^k remain positive and bounded, the barrier parameter ν_k vanishes from above, and the inner tolerance ε_k is summable. The technical requirements and mild conditions for convergence are detailed, e.g., in [27]. The convergence properties of Algorithm 2.1 can be analyzed with the lens of inexact proximal point algorithms; we refer the interested reader to [9, 30, 11, 10, 26, 21, 5, 4] for recent results established by exploiting this connection for regularized QP solvers.

2.2 Inner minimization with Newton

The minimization procedure adopted to solve the subproblem at Step 5 of Algorithm 2.1 is typically based on Newton’s method with a backtracking line search procedure for globalization. Methods of this kind for convex unconstrained minimization have been extensively studied and provide strong convergence guarantees. However, a direct application of Newton method to minimize \mathcal{M}_k is usually deemed impractical and avoided, since the Hessian matrix $\nabla^2 \mathcal{M}_k$ tends to be dense. However, by convexity of \mathcal{M}_k , it is sufficient to find a zero of $\nabla \mathcal{M}_k$. Using the linear transformation T_{δ^k} in [10, §3.1], we can obtain an equivalent root-finding subproblem that retains structure and sparsity of the original problem (1):

$$0 = T_{\delta^k} \nabla \mathcal{M}_k(x, s, y, z) = \begin{pmatrix} Qx + q + A^\top y + G^\top z + \delta_{x,k}(x - \theta_x^k) \\ -\frac{\nu_k}{s} + z \\ Ax - b + \delta_{y,k}(\theta_y^k - y) \\ Gx - d + s + \delta_{z,k}(\theta_z^k - z) \end{pmatrix}. \quad (8)$$

Scaling the second block by $s > 0$, the classical primal-dual IP subproblem is recovered with additional proximal regularization terms, as in [30, §2], [9, §3]. Then, at any point (x, s, y, z) , a Newton direction $(\Delta x, \Delta s, \Delta y, \Delta z)$ can be obtained by solving the following system of linear equations:

$$\begin{bmatrix} Q + \delta_{x,k} \mathbb{I}_n & 0 & A^\top & G^\top \\ 0 & \text{diag}(z) & 0 & \text{diag}(s) \\ A & 0 & -\delta_{y,k} \mathbb{I}_m & 0 \\ G & \mathbb{I}_p & 0 & -\delta_{z,k} \mathbb{I}_p \end{bmatrix} \begin{pmatrix} \Delta x \\ \Delta s \\ \Delta y \\ \Delta z \end{pmatrix} = - \begin{pmatrix} Qx + q + A^\top y + G^\top z + \delta_{x,k}(x - \theta_x^k) \\ -\nu_k + s \odot z \\ Ax - b + \delta_{y,k}(\theta_y^k - y) \\ Gx - d + s + \delta_{z,k}(\theta_z^k - z) \end{pmatrix}, \quad (9)$$

for which there exist several numerical techniques; see e.g. [15] for an overview. In (9), \mathbb{I}_n denotes the identity matrix of size n , $\text{diag}(s)$ builds a square diagonal matrix with diagonal s , and \odot indicate the Hadamard product. As our focus is on the combination of the optimization routine in Algorithm 2.1 with a learning-based hyperparameter policy, the (sparse) linear system (9) is solved directly through LU decomposition with pivoting, for numerical stability, without any additional structure exploitation. It is worth mentioning here that the regularization parameters δ are introduced as penalty weights in the definition (5) of the augmented Lagrangian, with the goal of discouraging constraint violations, but they also play an important role in mitigating the ill-conditioning of matrices arising from the IP scheme; cf. [9, §4].

2.3 Hyperparameters

The behavior and performance of Algorithm 2.1 depend on the sequences of hyperparameters $\{\delta^k\}$, $\{\nu_k\}$ and $\{\varepsilon_k\}$. As depicted in Figure 1, we deliberately consider the barrier parameter ν and inner tolerance ε as endogenous hyperparameters; their values are selected by evaluating common heuristic rules. Conversely, the regularization parameters δ will be subject to the action of the external RL agent and updated according to its policy.

Given a user-defined tolerance $\epsilon > 0$, the sequence of barrier parameters is generated according to $\nu_{k+1} = \max\{\epsilon/10, \min\{\kappa_\nu \nu_k, \nu_k^{\theta_\nu}\}\}$ as in Ipopt [39, Eq. 7], starting from $\nu_0 = 1$ and with linear factor $\kappa_\nu \in (0, 1)$ and superlinear factor $\theta_\nu \in (0, 1)$; see Table 2. Analogously, the inner tolerance ε evolves as $\varepsilon_{k+1} = \max\{\epsilon/10, \kappa_\varepsilon \alpha_\varepsilon^k \varepsilon_k\}$ with decay rate $\kappa_\varepsilon \in (0, 1)$ and decay damping $\alpha_\varepsilon \in (0, 1)$. The initial inner tolerance ε_0 is chosen adaptively, based on the primal-dual guess (x^0, s^0, y^0, z^0) according to $\varepsilon_0 = \xi \|\nabla \mathcal{M}_0(x^0, s^0, y^0, z^0)\|_2$, where $\xi \in (0, 1)$ is the initial damping factor.

While parameters ν and ε should become sufficiently small, there is no clear way to choose the weights δ ; in fact, convergence is guaranteed even if they are kept constant. This motivated us to experiment

with machine learning techniques to discover a “good” policy for updating δ^k . Our approach is to define the update rule as

$$\delta_{\square,k+1} = \max\{\delta_{\min}, \alpha_{\square,k} \delta_{\square,k}\} \quad \text{for } \square \in \{x, y, z\}, \quad (10)$$

starting from some $\delta^0 = (\delta_{x,0}, \delta_{y,0}, \delta_{z,0}) \in \mathbb{R}_{++}^3$, where the small threshold $\delta_{\min} > 0$ safeguards the numerical linear algebra for (9) and the decrease factors $\alpha_{\square,k} \in (0, 1)$ are outputs of the RL policy; see Figure 1. To fix ideas, the RL action takes the form

$$\alpha^k = \begin{pmatrix} \alpha_{x,k} \\ \alpha_{y,k} \\ \alpha_{z,k} \end{pmatrix} = \alpha(r_{\text{prim}}(x^k, y^k, z^k), r_{\text{dual}}(x^k, y^k, z^k), \nu_k, \varepsilon_k), \quad (11)$$

where the mapping α is learned by training a neural network π_{ζ} . The choice of defining this mapping with residuals as inputs, as opposed to primal-dual decision variables (x, y, z) , is intended to make the mapping invariant to the problem dimensions (n, m, p) ; subsequently we will make it also scale-invariant.

We conclude this overview on the QP solver by remarking that common safeguards and tricks for numerical stability were intentionally left out. Therefore, features such as boundary control [30], centrality correction [36], presolving and Ruiz-based preconditioning [37], nonmonotone line search [20], and adaptive early-termination strategies are deactivated for all numerical tests. Our intention is twofold, and opposed to displaying state-of-the-art performance: (i) leaving the numerical noise and issues unfiltered to stress the solver and (ii) providing a clean baseline to isolate and analyze the effect of RL on the performance.

3 Learning-enhanced methods

In the following, we aim at finding a good strategy to choose the parameters during the optimization. So far, the choice of these parameters is up to the operators, and thus, the optimization highly depends on their experiences. Reinforcement learning [38] makes it possible to automate this choice and avoid manual hyperparameter tuning. Therefore, reinforcement learning approaches benefit from their ability to train a policy by interacting with the environment in a trial-and-error manner. In recent years, the use of machine learning methods in order to improve optimization strategies has increased. For example, neural networks are used to warm-start either QPs [33] or Fixed-Point Optimization Algorithms [34].

In [22] the authors apply a Twin-Delayed Deep Deterministic Policy Gradient approach to adapt step size parameters for solving QP problems. But instead of improving the Alternating Direction Method of Multiplier (ADMM) approach, we focus on the regularized interior point approach, which was discussed earlier. Thus, the goal is to automate the choice of parameters $\alpha_{\square,k}$ for $\square \in \{x, y, z\}$ in iteration k . Thereby, the choice should be made with respect to the primal and dual residuals, the barrier parameter and the inner tolerance as in (11). Figure 1 shows the embedding of the RL policy into the optimizer which is summarized in Algorithm 2.1. In an inner loop, the primal-dual augmented Lagrangian function $\mathcal{M}_{\delta}(x, s, y, z; \theta, \nu)$ is minimized for fixed θ^k , barrier parameter ν_k and weights $\delta_{\square,k}$ until a tolerance ε_k is reached. Once this has been achieved, in an outer loop θ^k , ν_k and ε_k are updated for the next iteration of the inner loop. In addition, the hyperparameters $\delta_{\square,k}$ are adapted by factors $\alpha_{\square,k}$, which are determined by the RL policy. Thus, the RL policy acts at Step 3 in Algorithm 2.1, where δ^k is updated. This procedure is repeated until the primal and dual residuals are small enough. During training, the policy to be learned is improved step by step by interacting with the described framework, which in RL context is also called “environment”, while trying to solve randomly selected QPs.

3.1 State and reward

We continue with the mathematical background, which is needed for Reinforcement Learning. RL is based on the Markov decision process (MDP) [13], which is represented by the quadruple $(\mathcal{S}, \mathcal{A}, \mathcal{P}, \mathcal{R})$. The state space \mathcal{S} comprises all possible configurations of the environment, while the action space \mathcal{A} represents all actions which allow the policy to influence the environment. The probability transition \mathcal{P} describes the probability of reaching a state under the condition that the previous state and action are given. Finally, the reward function $\mathcal{R} : \mathcal{S} \times \mathcal{S} \rightarrow \mathbb{R}$ rates the state transition and enables to compare and improve solutions. While the state and action space as well as the reward function need to be defined

by the operator, the probability transition does not need to be given explicitly. It is compensated by the interaction of the policy with the environment. In the following, we will define this framework for our present task.

State Since we are convinced that the choice of factors $\alpha_{\square,k}$ for $\square \in \{x, y, z\}$ depends mainly on the primal and dual residuals of the QPs, we decide to make them part of the state definition. Moreover, since the residuals (r_{prim} and r_{dual}) can span several orders of magnitude during the solution process, causing scaling issues while training the policy networks, we encode the environment state with residuals in logarithmic scale:

$$\sigma(x, y, z, \nu, \varepsilon) := \begin{pmatrix} -\log(\sigma_{\text{prim}}(x, y, z) + 10^{-9}) \\ -\log(\sigma_{\text{dual}}(x, y, z) + 10^{-9}) \\ -\log(\nu + 10^{-17}) \\ -\log(\varepsilon + 10^{-9}) \end{pmatrix} \quad (12)$$

where the normalized residuals σ_{prim} and σ_{dual} defined by

$$\sigma_{\text{prim}}(x, y, z) := \frac{r_{\text{prim}}(x, y, z)}{\max\{\|A\|_{\infty}, \|b\|_{\infty}, \|G\|_{\infty}, \|d\|_{\infty}\}} \quad (13a)$$

$$\sigma_{\text{dual}}(x, y, z) := \frac{r_{\text{dual}}(x, y, z)}{\max\{\|Q\|_{\infty}, \|q\|_{\infty}, \|A\|_{\infty}, \|G\|_{\infty}\}} \quad (13b)$$

are intended to make the state definition scale-invariant.

Remark: The inclusion of the barrier parameter ν and tolerance ε into the state vector guarantees the Markov property of our framework. Note that at this point our choice of the state vector differs from the one chosen in [22], which did not have any additional parameters that need to be updated for an inner loop. In our case, omitting them would have made it necessary to introduce a partially observable MDP [23]. However, the preliminary numerical tests reported in Section 4 indicate that the RL training remains manageable and efficient in practice. Nevertheless, an extension to partially observed MDPs associated with a change of RL formulation seems of interest for an even leaner training procedure, but it comes with challenges and is left for future research.

Action The action of our task is the choice of $\alpha_{\square,k}$ in each iteration step k for $\square \in \{x, y, z\}$. Since $\alpha_{\square,k}$ is the factor that is used to sequentially decrease the regularization parameter $\delta_{\square,k}$, according to (10), it must be strictly positive and smaller than or equal to one.

Reward Finally, we define the reward function. We remember that our goal was to accelerate the interior point approach. To achieve this, we define a reward function, which consists of three parts

$$\mathcal{R}(\sigma, \sigma') := \mathcal{R}_1(\sigma, \sigma') + \mathcal{R}_2(\sigma, \sigma') + \mathcal{R}_3(\sigma, \sigma') \quad \text{for } \sigma, \sigma' \in \mathcal{S}, \quad (14)$$

where each term depends on the scaled residuals $\sigma_{\text{prim}}(x, y, z), \sigma_{\text{dual}}(x, y, z)$ and the inner-loop iteration count N required to meet the early-termination tolerance.

The first component, \mathcal{R}_1 , penalizes imbalance between primal and dual residuals. As shown in Figure 1 and Algorithm 2.1, the method combines inner- and outer-loop updates. To validate early termination at tolerance ε , both residuals must be simultaneously small, which enforces a tube along the axis $r_{\text{prim}} = r_{\text{dual}}$. The tube behavior is shown in Figure 6. We define

$$\mathcal{R}_1(\sigma, \sigma') := -\tanh\left(\left|\log(\sigma'_{\text{prim}} + 10^{-9}) - \log(\sigma'_{\text{dual}} + 10^{-9})\right| \cdot c_g\right). \quad (15)$$

The definition of c_g and other constants that appear in the reward are listed in Table 4.

The second component, \mathcal{R}_2 , rewards large reductions in the residuals between consecutive outer loops, thereby promoting consistent improvement in feasibility and optimality before updating the proximal and augmented Lagrangian parameter δ_{\square} . It is given as

$$\begin{aligned} \mathcal{R}_2(\sigma, \sigma') := & \tanh\left(\left(\log(\sigma_{\text{prim}} + 10^{-9}) - \log(\sigma'_{\text{prim}} + 10^{-9})\right) \cdot c_p\right) \\ & + \tanh\left(\left(\log(\sigma_{\text{dual}} + 10^{-9}) - \log(\sigma'_{\text{dual}} + 10^{-9})\right) \cdot c_p\right). \end{aligned} \quad (16)$$

The third component, \mathcal{R}_3 , provides a performance bonus scaled by the iteration budget c_{perf} , incentivizing rapid convergence within a limited number of steps. For the inner-loop iteration count $N \in \mathbb{N}_{>0}$, the third component reads

$$\mathcal{R}_3(\sigma, \sigma') := 1 - \exp\left(-\frac{N}{c_{\text{perf}}}\right). \quad (17)$$

Note that the terms \mathcal{R}_1 and \mathcal{R}_2 are smoothed by hyperbolic tangent functions, bounding them in $[-c_g, c_g]$ and $[-c_p, c_p]$, respectively. The parameter c_{perf} determines the maximum negative value attainable by \mathcal{R}_3 .

Neural network After we have defined the MDP, all that remains is to define the policy in order to have an RL framework. Our parameterized policy π_ζ is represented by a feedforward neural network, whose weights and biases form the parameters ζ . We determined the size of the network by a grid search and decided on a net with two hidden layers, each containing 25 neurons. The size of the input layer (four) and output layer (three) are given by the dimension of the state and action space. For each layer, the hyperbolic tangent is used as the activation function.

Based on these definitions, RL aims to maximize the objective with respect to the weights and biases of the neural network:

$$\min_{\zeta} \quad \mathbb{E} \left[\sum_{i=0}^{\infty} \gamma^i \mathcal{R}(\sigma_i, \sigma_{i+1}) \right]$$

with discount factor $\gamma \in (0, 1)$ and $\sigma_i \in \mathcal{S}$ for $i \in \mathbb{N}$. Note that the expected value, which appears in the objective function, is defined over all trajectories $(\sigma_0, \alpha_0, \sigma_1, \alpha_1, \dots)$ for $\alpha_i \in \mathcal{A}$.

3.2 Training procedures

Based on the MDP, which was defined in the previous subsection, we run the RL approach. We chose Proximal Policy Optimization (PPO) [35], as it is considered robust and stable and is capable of handling continuous action spaces. It is an actor-critic RL approach, which means that the policy π_ζ and the value function V_Φ with parameters Φ are trained simultaneously. Note that in our case, both the policy and the value function share the majority of the neural network, which was described before. Typically, PPO uses an approximation of the advantages function \hat{A}_k in iteration $k \in \mathbb{N}$, which has the form:

$$\hat{A}_k := \sum_{i=0}^{\infty} (\gamma\lambda)^i (\mathcal{R}(\sigma_{k+i}, \sigma_{k+i+1}) + \gamma V_\Phi(\sigma_{k+i+1}) - V_\Phi(\sigma_{k+i})).$$

For the parameter, which is used for the general advantage estimation \hat{A}_k , it holds $\lambda \in [0, 1]$. Now, the parameters of the policy can be updated. For the update, a gradient ascent of the following objective function for $\tau \in [0.1, 0.3]$ is computed:

$$L_\pi(\zeta) = \mathbb{E}_k \left[\min \left(\frac{\pi_\zeta(\alpha_k | \sigma_k)}{\pi^{\text{old}}(\alpha_k | \sigma_k)} \hat{A}_k, \text{clip} \left(\frac{\pi_\zeta(\alpha_k | \sigma_k)}{\pi^{\text{old}}(\alpha_k | \sigma_k)}, 1 - \tau, 1 + \tau \right) \hat{A}_k \right) \right].$$

It is based on the idea that the quotient of the new policy π_ζ and the previous policy π^{old} becomes larger in the case of a positive advantage value and smaller otherwise. Furthermore, the objective function is clipped if the policy update becomes too intense, leading to a more robust training. After the policy update, the approximation of the value function V_Φ is updated by a gradient descent of the loss function:

$$L_V(\Phi) := \frac{1}{2} \mathbb{E}_k \left[(V_\Phi(\sigma_k) - \mathcal{R}(\sigma_k, \sigma_{k+1}) - \gamma V_\Phi(\sigma_{k+1}))^2 \right].$$

Our technical implementation is based on the RL library **RLlib** [25, 41]. The choice of hyperparameters for the described PPO approach can be seen in Table 1.

As metric to monitor the training, we observe the policy loss, the value function loss and the entropy in each episode. The loss value trends show the training behavior of the policy and the value function. The entropy is monitored, since it represents the exploration and uncertainty of the policy during the training.

Learning rate schedule	(0, $5 \cdot 10^{-4}$)	Entropy coeff. schedule	(0, $5 \cdot 10^{-4}$)
	(500K, $3 \cdot 10^{-4}$)		(1M, $3 \cdot 10^{-4}$)
	(1M, 10^{-4})		(2M, 10^{-4})
	(2M, $5 \cdot 10^{-5}$)		
	(3M, 10^{-5})		
	(4M, $5 \cdot 10^{-6}$)		
	(5M, 10^{-6})		
	(7M, $5 \cdot 10^{-7}$)		
	(9M, 10^{-7})		
	(20M, 10^{-8})		
Batch size	4096	γ	0.99 (default)
λ	1.0 (default)	ϵ	0.2 (default)
Gradient clip	25	KL coeff.	0.05
KL target	0.01	Network layers	[25, 25] (tanh)
Num. CPUs (local worker)	20	Num. CPUs per worker	1
System configuration	Kubuntu 22.04.5 LTS Intel Core i9-12950HX		

Table 1: PPO hyperparameters used in training.

ϵ	κ_ϵ	α_ϵ	ξ	κ_ν	θ_ν	max-outer-it
10^{-6}	0.5	0.98	10^{-2}	0.2	1.5	25
δ_{\min}	$\delta_{x,0}$	$\delta_{y,0}$	$\delta_{z,0}$	α_{\min}	α_{\max}	max-inner-it
10^{-12}	1	10	10	0.05	0.95	25

Table 2: Default solver setup.

For the training and numerical experiments reported in this work, the solver is configured as summarized in Table 2. The superlinear barrier decrease is governed by $\kappa_\nu = 0.2$ and $\theta_\nu = 1.5$, as in Ipopt [39]. The tolerance ϵ for the termination conditions (3) is set to 10^{-6} . The early-termination decay rate is initialized at $\kappa_\epsilon = 0.5$ and progressively damped at each outer iteration by a factor $\alpha_\epsilon = 0.98$. An additional initialization parameter is set to $\xi = 0.01$.

3.3 Training problem set

Random QP problems are generated to train the Reinforcement Learning loop illustrated in Figure 1. Each problem of the form (1) is defined by matrices Q, A, G and vectors q, b, d , with properties such as convexity, sparsity, LICQ (Linear Independence Constraint Qualification), and conditioning carefully controlled to produce meaningful and diverse problem batches. Matrix Q encodes the convexity and conditioning of the problem and is constructed as $Q = W^\top W$, where W is a random matrix that always has rank deficiency. The sparsity of Q is determined by the sparsity of W . Specifically, the number of nonzeros in Q depends on how the nonzero rows and columns of W interact. The density of W is $\frac{\text{nnz}(W)}{hn} \in (0, 1)$. For each batch of problems, an average number of nonzero entries per row, nnz_{row} , for W is sampled from a bounded uniform distribution, see Table 3. Note that the density of Q is always greater than the one of W and may vary depending on the structure of W . This approach introduces variability in sparsity patterns across the batch, covering a wide range of problem constructions.

Non-strict convexity Due to the rank deficiency of $W \in \mathbb{R}^{h \times n}$, $h < n$, the $Q \in \mathbb{R}^{n \times n}$ matrices of the batches are always symmetric positive semi-definite, and not positive definite, resulting in non-strictly convex QPs. The used rank deficiency of W is set to $n/2$.

Constraints linear dependencies Numerical challenges arise for Newton-type solvers when dealing with equality and inequality constraints (1) that are linearly dependent, because of singular linear systems. In practice, we generate m equality and p inequality constraints and then a fraction of constraints, $m/2$ and $p/2$, is duplicated and thus linearly dependent, increasing the total number of constraints to $3m/2$.

and $3p/2$. These linear dependencies make the KKT matrix singular and, when solving (9) the linear system solver struggles due to an ill-posed linear system at each iteration. The augmented Lagrangian formulation using δ_y, δ_z breaks this linear dependency and regularizes the problem.

Ill-conditioning QP problems can become numerically challenging when Q is ill-conditioned, as this directly affects the conditioning of the KKT matrix (9) and the accuracy of the linear solver in each Newton step. When the condition number of the linear systems (9) is high, small numerical errors are amplified during LU or Cholesky factorization, making the Newton directions inaccurate and slowing down convergence, or breaking it altogether. In our training set, the condition number of the Q matrices is explicitly controlled.

For this purpose, we use the following considerations. As Q is positive semi-definite, all eigenvalues of Q are non-negative but some are equal to zero. Thus, we focus on the effective condition number κ_e

$$\kappa_e(Q) := \frac{\lambda_{\max}(Q)}{\lambda_{\min,+}(Q)}, \quad (18)$$

where $\lambda_{\max}(Q)$ represents the largest eigenvalue of Q while the smallest positive eigenvalue of Q is named $\lambda_{\min,+}(Q)$. Furthermore, since $Q = W^\top W$, we have $\lambda_{\max}(Q) = \sigma_{\max}^2(W)$ and $\lambda_{\min,+}(Q) = \sigma_{\min,+}^2(W)$, with $\sigma_{\max}(W)$ and $\sigma_{\min,+}(W)$ the largest and the smallest positive singular values of W . Consequently, the effective condition number of Q can be expressed as

$$\kappa_e(Q) = \left(\frac{\sigma_{\max}(W)}{\sigma_{\min,+}(W)} \right)^2. \quad (19)$$

Overall, to control $\kappa_e(Q)$, a target condition number $\kappa_Q^{\text{target}} \sim \mathcal{U}^{\log}(10^{15}, 10^{20})$ for Q is drawn. Afterwards, we manipulate the singular values of W by scaling its columns up to the drawn κ_Q^{target} according to a geometric sequence. Particularly, the scaling is applied to each column $W_{:,j}$ as

$$W_{:,j} \leftarrow \left(\frac{1}{\sqrt{\kappa_Q^{\text{target}}}} \right)^{\frac{j-1}{n-1}} W_{:,j}, \quad \forall j = 1, \dots, h, \quad h < n, \quad (20)$$

thereby imposing an approximate singular value decay on Q and controlling its ill-conditioning to the desired level.

Initial guess control It is essential that the training dataset covers a broad range of the state space to ensure that Algorithm 2.1 encounters diverse scenarios during convergence. Coverage can be improved by strategically selecting initial points while keeping generation costs low. If initial points are consistently chosen near feasibility and stationarity, the residuals $(r_{\text{prim}}, r_{\text{dual}})$ will exhibit limited variation, biasing the training distribution toward nearly optimal states. To avoid this, candidate initial solutions (x, y, z) are selected such that the initial residuals satisfy $r_{\text{prim}}^{\text{target}}, r_{\text{dual}}^{\text{target}} \sim \mathcal{U}^{\log}(10^{-2}, 10^2)$ and are found by solving a least-squares problem. The variable x is randomly generated, and the vectors b and d are constructed to enforce the primal residual as

$$b = Ax + r_{\text{prim}}^{\text{target}} \quad \text{and} \quad d = Gx + r_{\text{prim}}^{\text{target}} + \mu, \quad (21)$$

where μ is a random positive value ensuring the inequality direction. Then, with fixed x , the unregularized dual residual $r_{\text{dual}}^{\text{target}}$ can be obtained by solving the least-squares problem

$$\arg \min_{y,z} \|Qx + q + A^\top y + G^\top z - r_{\text{dual}}^{\text{target}}\|_2^2 \quad \text{subject to} \quad z \geq 0 \quad (22)$$

from which the multipliers y and z are computed. In practice, solving the constrained problem (22) is computationally expensive for large-scale dataset generation. Therefore, the unconstrained counterpart is solved and the inequality multipliers z are then projected onto the nonnegative orthant.

The training and validation datasets are summarized in Table 3, which reports the ranges and distributions of the problem dimensions, the controlled effective condition number of Q , and the sparsity

Setup	n	m	$\frac{n}{\overline{\mathcal{U}(2,5)}}$
Training	$\mathcal{U}(20, 30)$	p	$n\mathcal{U}(2, 5)$
Validation	$\mathcal{U}(20, 30)$	$\text{nnz}_{\text{row}}(W)$	$\mathcal{U}(2, 5)$
Scale $10\times$	$\mathcal{U}(200, 300)$	$\kappa_e(Q)$	$\mathcal{U}^{\log}(10^{15}, 10^{20})$

Table 3: Setup to build random QPs for training and validation sets.

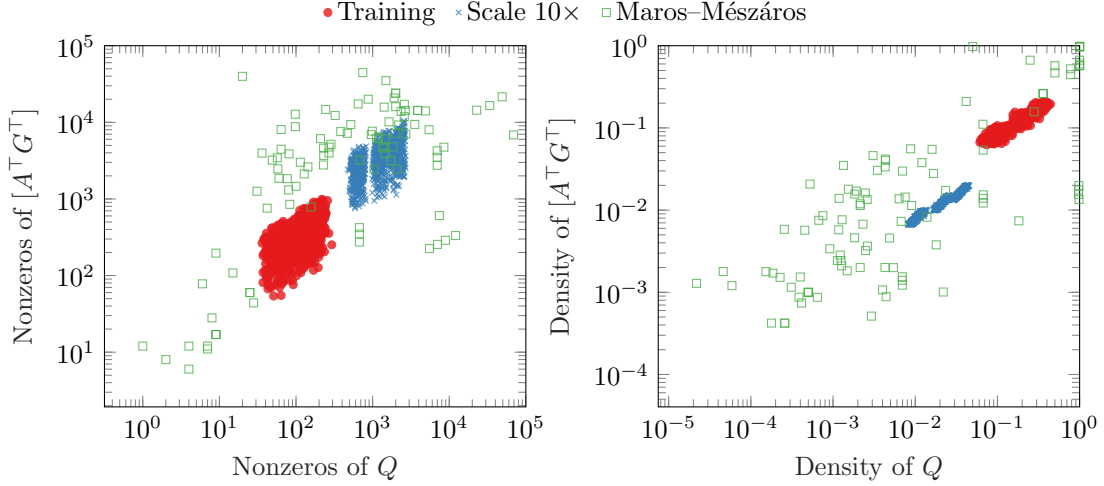


Figure 2: Distribution of problem size (in terms of number of nonzero entries) and density for randomized training, validation, and scale $10\times$ problems (sample of 10^3 instances) and for Maros-Mészáros problems (100 smallest instances).

pattern per row of the matrix W . These settings are used to generate random QPs for both training and validations.

Figure 2 presents the actual problem sizes and sparsity statistics for the generated datasets, including the number of variables, constraints, and the distribution of nonzeros per row in the constraint matrices. For reference, the figure also includes a comparison with the problem sizes and sparsity patterns from the Maros-Mészáros benchmark set. The training random problems exhibit a broad range of nonzero values in Q and $[A^T G^T]$, which are further scaled by a factor of $100\times$ in the scale $10\times$ validation set. In terms of sparsity, these generated problems maintain a consistent patterns across the dataset. In contrast, the Maros-Mészáros benchmark test set displays a wider diversity in both the number of nonzeros and the sparsity patterns, making it challenging to solve as a batch using a single solver configuration.

The targeted versus actual residuals for the generated problems are illustrated in Figure 3, highlighting the effectiveness of the initial candidate generation procedure in achieving the desired residual ranges. While the primal and dual residuals exhibit larger errors in the range $[10^{-2}, 1]$ (i.e., closest to the solution), the control performs well for larger residual values. The objective of the method is not high precision, but rather to ensure a diverse coverage of initial residuals at low computational cost.

4 Numerical investigations

We report the outcomes of the training process and corresponding validation, followed by an evaluation on larger randomly generated problems to assess scalability. Finally, we benchmark the approach on the Maros-Mészáros test set to examine its zero-shot generalization on challenging real-world problem instances. The analysis is based on performance and data profiles, consistently comparing the RL-enhanced solver with the typical fixed- α strategy. The robustness and acceleration of the different methods will be discussed in the analysis.

Profiles For P the set of problems and S the set of solvers, let $t_{s,p}$ denote the (wall-clock) runtime required by solver $s \in S$ to solve instance $p \in P$ (for a given tolerance $\epsilon > 0$). We will monitor the

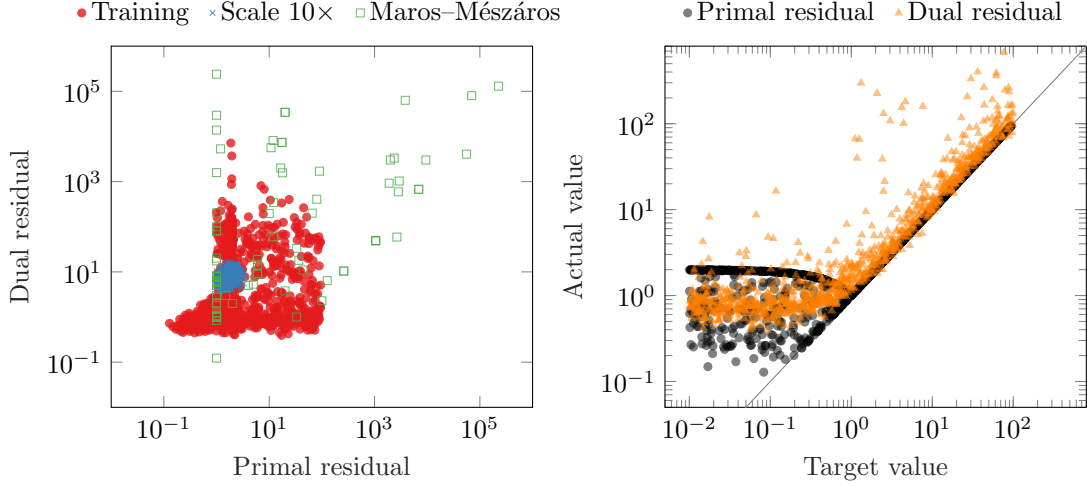


Figure 3: Distributions of problem initial residuals (sample of 10^3 instances). Primal-dual values for different problem classes (left panel). Target vs actual values generated for the training procedure (right panel).

computational performance of different solver settings and graphically summarize our results by means of two profiles. When solver $s \in S$ fails to solve $p \in P$, we set $t_{s,p} = \infty$.

- A *data profile* is the graph of the cumulative distribution function $f_s: [0, \infty) \rightarrow [0, 1]$ of the runtime, namely $f_s(t) := \frac{|\{p \in P \mid t_{s,p} \leq t\}|}{|P|}$, where $|P|$ denotes the cardinality of set P . As such, each data profile reports the fraction of problems $f_s(t)$ that can be solved by s with a computational budget t , and therefore it is independent of the other solvers.
- A *performance profile* is the graph of the cumulative distribution function of the performance ratio $r_{s,p} := \frac{t_{s,p}}{\min_{s' \in S} t_{s',p}}$. As such, it displays the fraction of problems solved within a time factor compared to the fastest solver of each problem. Therefore, the performance profile of a solver also depends on the performance of all other solvers in S .

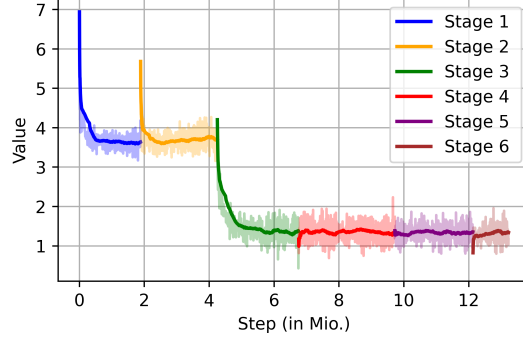
4.1 Training results

The reward parameters are presented in Table 4 from stage 1 to 6, respectively displayed with different colors in Figure 4. The first training stage have only \mathcal{R}_1 and \mathcal{R}_2 and the goal here is to create a sane structure for the neural network and a smooth mapping $\sigma(x, y, z, \nu, \varepsilon) \rightarrow \alpha$. The second stage incorporate all rewards term and introduce first the performance term, acting on the number of inner-loops which represent most of the solving time. The first and second reward term are required to ensure convergence of the primal-dual solver by promoting sufficiently large outer-loop steps, preventing premature vanishing of δ_\square , and maintaining similarity between primal and dual residuals. Relying only on the performance term \mathcal{R}_3 would bias the training toward easier problems in average, where rapid decrease is sufficient and highly rewarded, while neglecting harder instances that demand a nontrivial δ_\square dynamics. In the final stages 3–6, only the performance term is retained, albeit at the risk of destabilizing the previously trained and structured neural network. The value of c_{perf} is set to 23 as a fast-tuning to bound \mathcal{R}_3 around $[0, -2]$ with a maximum allowed number of inner iteration of 25 and a maximum number of outer iteration set at 25; see Table 2 for the complete solver setup used for the training and validation set. The performance differences of the method after training stages 1, 2, 3 and 6 are shown in Figure 7. Stages 3–6 use the same reward formulation and are each run for at most 2 million steps; although identical, they are reported separately in the results to reflect how the experiments were conducted.

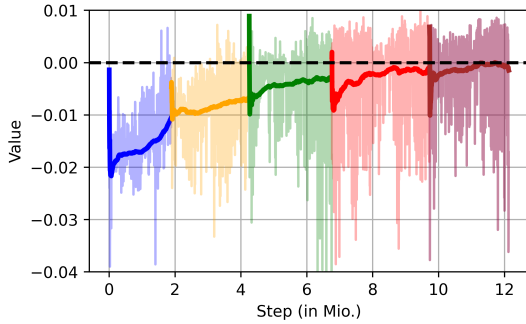
The training progress can be observed in Figure 4. In these figures, the different training phases (see Table 4) are indicated by different colors. In Figure 4a it can be observed how the loss of the critic evolves.

Training stage	c_g	c_p	c_{perf}
1	1	1	0
2	1	1	23
3 – 6	0	0	23

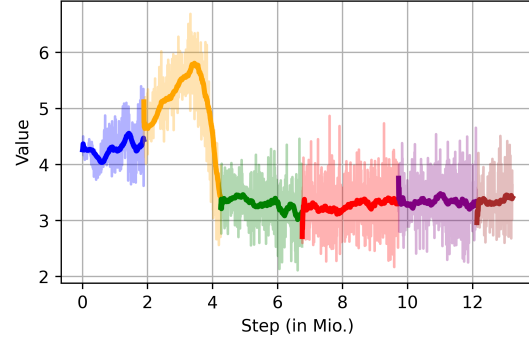
Table 4: Reward weights during the multistage training procedure.



(a) Value function loss



(b) Policy loss



(c) Entropy

Figure 4: Evolution of relevant metrics during the multistage training procedure.

Especially in the first three phases, a significant reduction of the loss can be noticed. This indicates that the approximation of the value function improves. In the last three phases, the PPO algorithm fine-tunes this approximation. The reason for the jumps of the loss function between phases lies in the change of the reward function, which is typical for curriculum learning. In addition to the loss function, Figure 4b shows the policy loss, which is an indicator of the improvement of the policy. The mostly negative values show that the policy improves, since advantageous actions, which means that they have a positive advantageous function approximation, are reinforced, and disadvantageous actions are weakened. Furthermore, we plot the entropy during training in Figure 4c. Entropy can be used to determine how uncertain or exploratory the training is. We see that the entropy increases in the first and second phases, which is a typical behavior, since exploration is needed at the beginning of the training. Afterwards, the entropy decreases and converges to a certain level. Although this behavior is common for RL algorithms in general, it is noticeable that the final level of the entropy is relatively high. This means that the final policy is relatively uncertain and is not close to a deterministic policy. The investigation of whether an enhanced state space or even longer training phases can make the policy more certain is left for future works. In any case, the plots indicate a successful training, and the influence of the RL policy on the QP solver is discussed in the remainder of this manuscript.

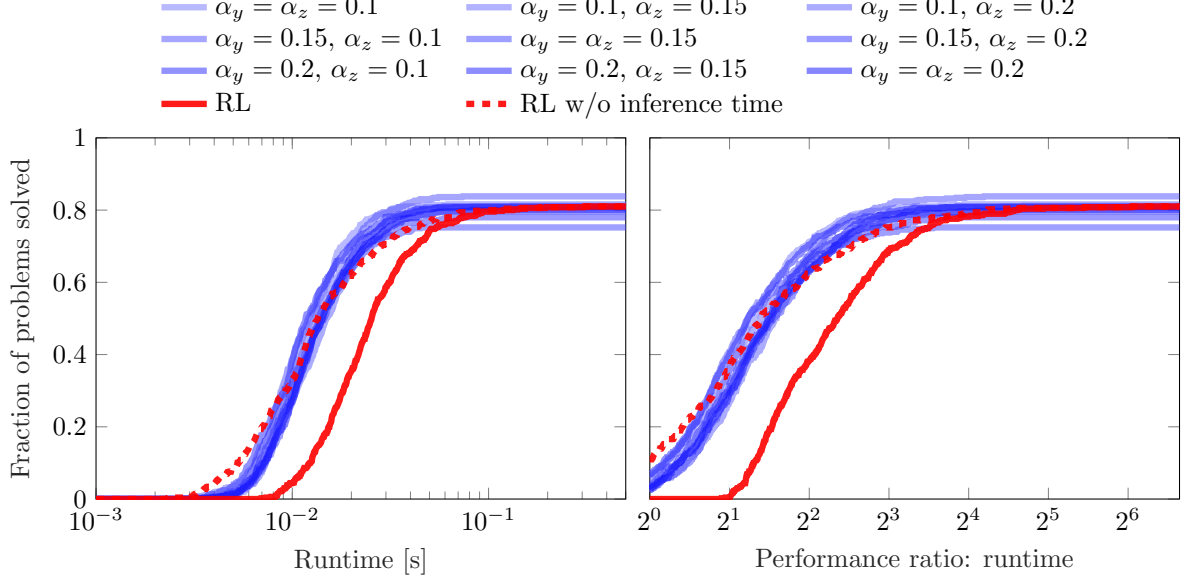


Figure 5: Validation set: Data (left) and performance (right) profiles comparing RL and solver configurations with fixed $\alpha_x = 0.15$, α_y and α_z .

4.2 Validation

After the multi-staged training, the performance of the method is evaluated on a batch of 4096 problems having the same properties as the problems used for the training, (see Table 3). In Figure 5, the performance and data profiles of the RL-enhanced solver are compared against different solver configurations with fixed α_{\square} values, which were obtained by extensive hand-tuning to achieve best performance. The fixed values of α_{\square} correspond to combinations of the values $\{0.1, 0.15, 0.2\}$. For these fixed settings, the robustness difference is about 10%, a significant margin for QPs, where state-of-the-art methods are already highly optimized and studied. The RL-enhanced solver is shown with its total runtime (red solid curve) and excluding the neural network inference time (red dashed line). Since the training problems are very small (see Table 3), the inference time of up to 0.1 seconds is non-negligible. The data profile (left panel) illustrates solving times ranging from 10^{-3} to 0.5 seconds, highlighting the diversity of problem complexity in the batch. In terms of performance, considering solving time only (dashed red line), the RL approach identifies sequences of $\alpha_{\square, k}$, $k \in \{0, 1, \dots, \text{max-outer-it}\}$ (and correspondingly δ_{\square}), enabling the solver to achieve the fastest solving times on approximately 25% of the test problems. In terms of robustness, the RL-enhanced method lies in the upper range of the tested solvers.

In Figure 6, the mapping $\sigma(x, y, z, \nu, \varepsilon) \rightarrow \alpha_{\square}$ is shown for fixed values $\nu = 10^{-2}$ and $\varepsilon = 10^{-2}$. The mappings are scaled by $-\log_{10}(\cdot)$, and can be read from the bottom-left corner to the upper-right corner, with a termination tolerance of $\epsilon = 10^{-6}$. The actions α_{\square} span the interval $[0.05, 0.95]$, ensuring a consistent decrease; see (10). This mapping still represents an early phase of the optimization process, and is typically observed after 4–5 outer iterations with good convergence (see κ_{ν} and θ_{ν} in Table 2). Consequently, noise is present for larger primal and dual residuals, since little to no data is available in these regions with the used early termination and the barrier parameter schedule. For the proximal weight δ_x decrease (left), very small values are obtained in the quadrant where the primal residual is smaller than the dual residual, while high values are observed in the opposite case. A smooth transition appears across the diagonal $r_{\text{prim}} = r_{\text{dual}}$. Within this region (“tube”) where primal and dual residuals are of similar magnitude, the values of α_{\square} fall within $[0.2, 0.5]$, which corresponds to the typical range used for fixed α -decrease schemes and serves as a useful benchmark for validating the RL-enhanced solver. For the equality-constraint weight δ_y (center), a simple pattern emerges, with α_y taking minimal values almost everywhere. This reflects the comparatively lower complexity of handling equality constraints relative to inequality constraints. For the inequality-constraint weight δ_z (right), a more intricate pattern is observed. The gradient forms a valley along the tube, where the values change more gradually than in the case of the proximal weight. Additionally, the symmetry along the “tube” of the α_x mapping is

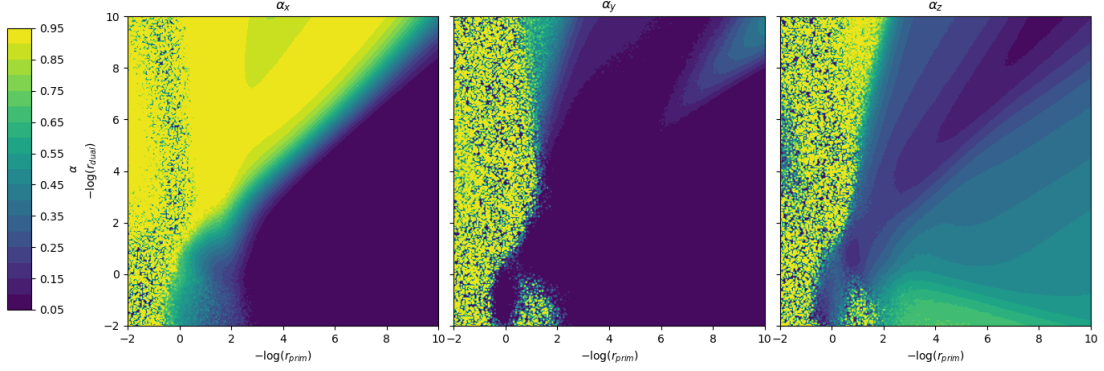


Figure 6: Mappings α_x (left), α_y (middle) and α_z (right): learned policy π_ζ evaluated with fixed $\nu = 10^{-2}$ and $\varepsilon = 10^{-2}$.

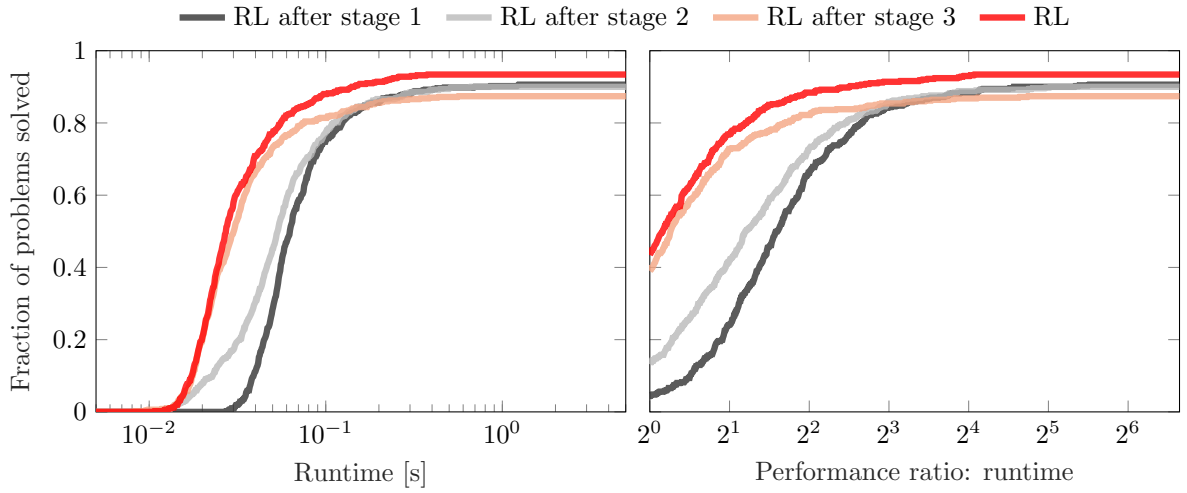


Figure 7: In-training validation: policy performance along the multistage process. Data (left) and performance (right) profiles comparing the influence of different RL policy.

reduced but still discernible.

4.3 Multistage learning and in-training validation

In Figure 7, the learned policies at training stages 1, 2, 3 and 6 performances are compared on the validation set (see Table 4). Between the first (black) and second (grey) stages, a substantial acceleration of the solving process is observed: the policy obtained after stage 2 consistently achieves faster solving times across all problems compared to stage 1. This improvement results from the introduction of the performance term in the reward, building on the stable neural network structure established during the first stage. On stage 3, where only the performance term is retained, the policy yields a further reduction in solving time but at the cost of approximately a 3% decrease in robustness. Continued training up to stage 6 produces the best results, with the final policy achieving both the fastest solving times and the highest robustness among the tested configurations.

4.4 Problem dimensions scaling

When evaluating the RL-policy on the validation set, the observed improvements over fixed α_\square strategies remain modest. This is largely due to the relatively small size of the validation problems, which, although ill-conditioned, non-strictly convex, and subject to redundant constraints, still exhibit limited complexity.

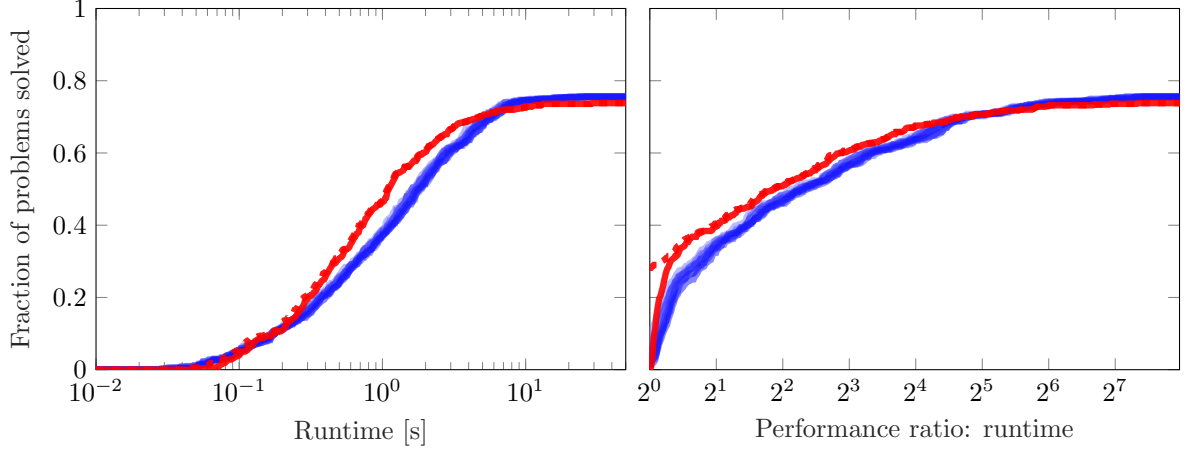


Figure 8: Scale $10\times$ set: Data (left) and performance (right) profiles comparing RL and solver configurations with fixed $\alpha_x = 0.15$, α_y and α_z .

However, the choice of random problem sizes during training (see Figure 2 for a comparison of problem properties) was primarily motivated by the need to keep the computational training cost low enough to complete on a personal computer within a single day; see the system configuration in Table 1. A question then arises: how does the policy π_ζ , trained at low cost, perform on larger problem instances?

Figure 8 presents the results for a batch of problems whose dimensions and sparsity are scaled by a factor of 10 relative to the validation set. As in the previous performance and data profiles, the solid red curve corresponds to the RL-enhanced solver, while the dashed red curve excludes the neural-network inference time. With larger problems, the inference overhead becomes negligible for the vast majority of cases (up to a performance ratio of 1.1). On these scaled problems, the RL-enhanced method solves most convergent instances faster than the standard geometric strategies across all tested α_\square -decrease schemes. Notably, its performance ratio reaches 2^4 for 80% of the problems (and 98% of those solved), underscoring the method’s ability to generalize and provide substantial gains on larger-scale instances.

4.5 Maros and Mészáros

Training was carried out on randomly generated problem instances, but an important question is how well the method generalizes to established benchmarks. To this end, we evaluate on the Maros–Mészáros test set [28], a widely used benchmark collection of challenging quadratic programs. This suite contains many large-scale and ill-conditioned problems and is considered a standard for assessing the robustness and efficiency of convex QP solvers. For evaluation, we consider the problem in a zero-shot generalization setting and focus on the 100 smallest instances (out of 138), where problem size is determined by folder size. A comparison of these instances with the randomly generated problems used for training is shown in Figure 2. As before, the Maros–Mészáros set is used in its raw form, meaning that inequality constraints with “infinite” bounds (represented as values of 10^{20} in OSQP [37]) are retained in the problem data (1). To accommodate the increased difficulty of these benchmarks, both the maximum number of inner and outer iterations are increased to 50.

The corresponding performance and data profiles are reported in Figure 9. The RL-enhanced solver is compared against fixed choices $\alpha_{x,y,z} = 0.1$, $\alpha_{x,y,z} = 0.2$, and $\alpha_{x,y,z} = 0.5$, both with and without accounting for neural-network inference time. The RL-enhanced solver demonstrates improvements in robustness of approximately 2%, 4%, and 7% relative to the fixed- α curves. As previously observed in the scale $10\times$ experiments, the RL-enhanced solver achieves speed-ups for problems requiring at least one second of solving time. When excluding inference time, its performance on the data profile matches the best fixed- α values for smaller problems solved in under 0.1 seconds. Although the Maros–Mészáros problems are not part of the training set, the RL solver identifies meaningful actions. Depending on the problem and solver configuration, finding an effective set of fixed α_\square values can be tedious, and both robustness and solution speed are highly sensitive to this choice. The test set is particularly diverse, with some problems solved in milliseconds and others requiring up to 30 seconds, making it challenging

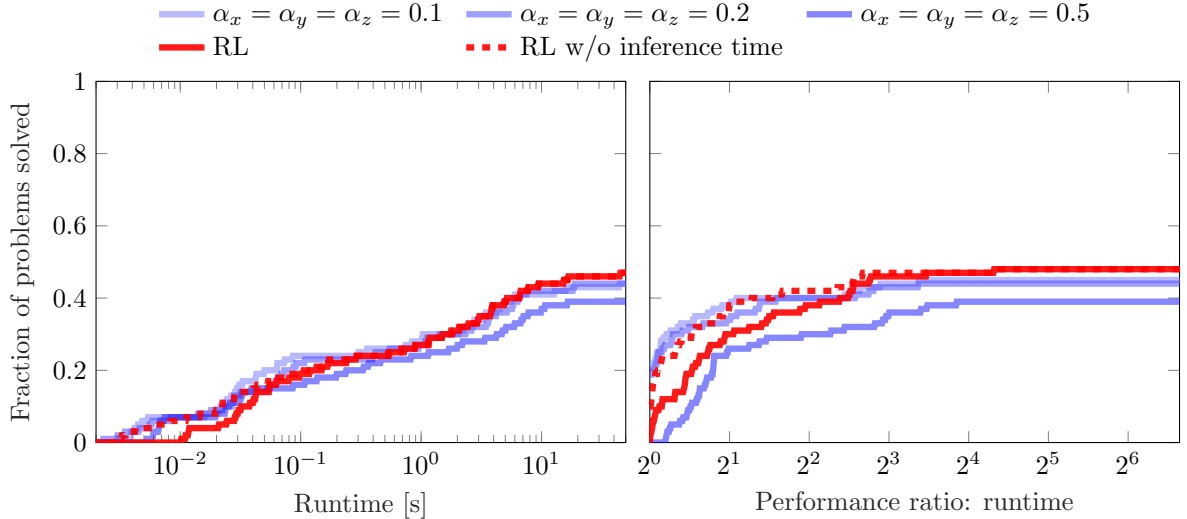


Figure 9: Maros–Mészáros set: Data (left) and performance (right) profiles comparing RL and solver configurations with fixed $\alpha_x = \alpha_y = \alpha_z$. Despite the lightweight training on random problems, the learned RL policy performs well on the previously unseen class of Maros–Mészáros instances.

to select a single fixed α_{\square} that performs well across the entire set. In contrast, the RL-enhanced method exhibits versatility, maintaining consistently high performance across the benchmark.

Depending on the problem’s conditioning and the choice of initial candidate, it may be beneficial for the user to tune the early-termination scaling factor ξ . This parameter determines the starting point for a fixed geometric decrease of ε_k and should be chosen consistently with the geometric decay rate α_{\square} to achieve the best performance.

Numerical results illustrating this effect are presented in Figure 10, where the RL-enhanced solver is evaluated for $\xi \in \{10^{-3}, 10^{-5}, 10^{-7}\}$ along with the default value $\xi = 10^{-2}$ for which the policy was trained. Even under a poorly chosen solver setup, the RL-enhanced solver adapts to maintain performance comparable to that obtained under a well-configured setup. Furthermore, all RL curves remain more robust than the fixed α_{\square} strategies, even when the latter are used with the best solver configuration ($\xi = 10^{-2}$). This versatility makes the solver more robust and easier to use, as it can automatically adapt to a wide range of problem instances. Examples include problems with large variations such as financial portfolio optimization, model predictive control under high perturbations and sudden noise and changes, large-scale power system optimization, trajectory planning for robotics in dynamic environments, and parameter estimation in ill-conditioned or highly constrained systems.

5 Final remarks and outlook

We presented a method based on reinforcement learning (RL) to speed up and harden the convergence of a (regularized Newton-based) solver for convex quadratic programming. We used RL to learn a policy aimed at adapting the solver’s hyperparameters to reduce the number of iterations needed to obtain a solution. For the RL training, we generated a framework to design small random QPs, which serves as good training problems. Then the parameterized RL policy, which is constructed as an artificial neural network, is trained on these QPs. In experiments, the results suggest that a single policy can improve convergence rates for a broad class of problems. In particular, we would like to emphasize the fact that the policy can successfully be used for problems with different sizes, scales and structures. Compared to previous approaches, like RLQP [22, §6], our lightweight training achieves similar validation performance with a fraction of time and memory (13 hours on a laptop vs. days on a high-end computer). Only for QPs that converge after few iterations, and thus require no hyperparameters adaptation, having a good neural policy is unnecessary at best. In these cases, the inference time it takes to evaluate the RL policy may reduce the performance benefit of faster convergence.

Despite these promising results, some questions remain for future works. For example, we will

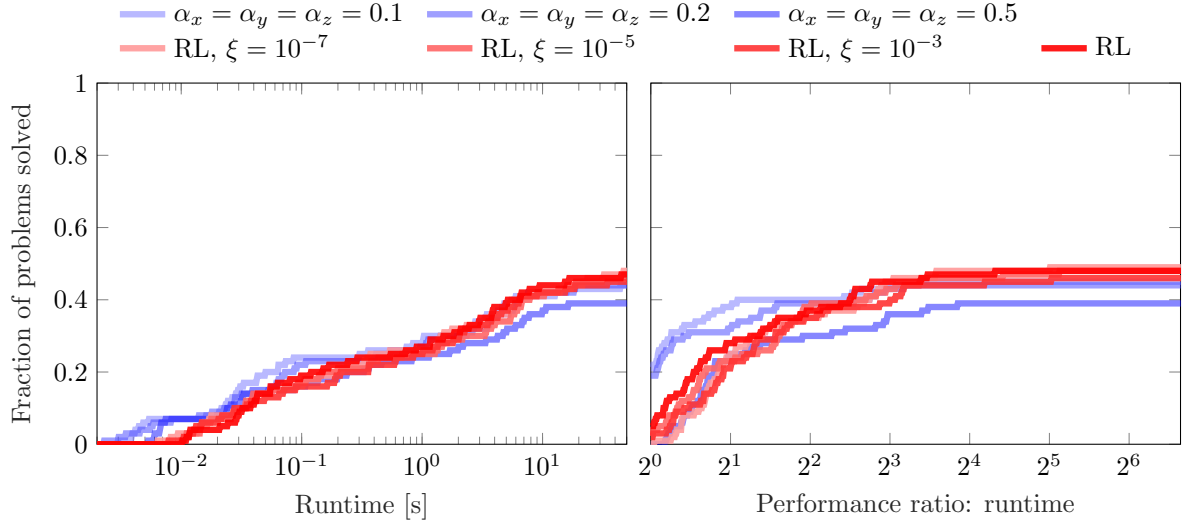


Figure 10: Maros–Mészáros set: Data (left) and performance (right) profiles comparing the influence of the RL policy on solver configurations with different values for ξ . The results with the default solver setup ($\xi = 10^{-2}$) and with fixed $\alpha_x = \alpha_y = \alpha_z$ are provided for comparison. The learned RL policy adapts well to different solver tuning, yielding consistent performance gains.

investigate whether additional RL policy options can further accelerate the convergence rate. Thereby, one aspect of investigation could be to measure the influence of the barrier parameter ν and the tolerance ε on the policy or the effect of including additional states, like the regularization parameter δ .

Furthermore, we will investigate the policy performance to other QP problem classes, such as large-scale sparse problems arising in power systems, optimal control problems showing particular three-banded structures or financial optimization with highly volatile market data. Moreover, for even more adaptive RL approaches, the policy could continue learning and improving during solver deployment. Lastly, it would also be valuable to benchmark the method against other state-of-the-art solvers, by extending with RL the in-house solver capable of solving the entire Maros–Mészáros test set.

References

- [1] B. Amos. Tutorial on amortized optimization, 2023, [2202.00665](#).
- [2] D. Applegate, M. Diaz, O. Hinder, H. Lu, M. Lubin, B. O’Donoghue, and W. Schudy. Practical large-scale linear programming using primal-dual hybrid gradient. In M. Ranzato, A. Beygelzimer, Y. Dauphin, P. Liang, and J. W. Vaughan, editors, *Advances in Neural Information Processing Systems*, volume 34, pages 20243–20257. Curran Associates, Inc., 2021. URL https://proceedings.neurips.cc/paper_files/paper/2021/file/a8fbbd3b11424ce032ba813493d95ad7-Paper.pdf.
- [3] C. Audet, K.-C. Dang, and D. Orban. Optimization of algorithms with OPAL. *Mathematical Programming Computation*, 6(3):233–254, 2014. doi:10.1007/s12532-014-0067-x.
- [4] A. Bambade, F. Schramm, S. El-Kazdadi, S. Caron, A. Taylor, and J. Carpentier. ProxQP: an efficient and versatile quadratic programming solver for real-time robotics applications and beyond. *IEEE Transactions on Robotics*, pages 1–19, 2025. doi:10.1109/TRO.2025.3577107.
- [5] A. Bemporad. A numerically stable solver for positive semidefinite quadratic programs based on nonnegative least squares. *IEEE Transactions on Automatic Control*, 63(2):525–531, 2018. doi:10.1109/TAC.2017.2735938.
- [6] E. G. Birgin and J. M. Martínez. Augmented Lagrangian method with nonmonotone penalty parameters for constrained optimization. *Computational Optimization and Applications*, 51(3):941–965, 2012. doi:10.1007/s10589-011-9396-0.
- [7] S. Boyd, N. Parikh, E. Chu, B. Peleato, and J. Eckstein. Distributed optimization and statistical learning via the alternating direction method of multipliers. *Foundations and Trends® in Machine Learning*, 3(1):1–122, 2011. doi:10.1561/22000000016.

- [8] R. Byrd, J. Nocedal, and R. Waltz. Feasible interior methods using slacks for nonlinear optimization. *Computational Optimization and Applications*, 26, 03 2002. doi:[10.1023/A:1025136421370](https://doi.org/10.1023/A:1025136421370).
- [9] S. Cipolla and J. Gondzio. Proximal stabilized interior point methods and low-frequency-update preconditioning techniques. *Journal of Optimization Theory and Applications*, 197(3):1061–1103, 2023. doi:[10.1007/s10957-023-02194-4](https://doi.org/10.1007/s10957-023-02194-4).
- [10] A. De Marchi. On a primal-dual Newton proximal method for convex quadratic programs. *Computational Optimization and Applications*, 81(2):369–395, 3 2022. doi:[10.1007/s10589-021-00342-y](https://doi.org/10.1007/s10589-021-00342-y).
- [11] A. De Marchi. Regularized interior point methods for constrained optimization and control. *IFAC-PapersOnLine*, 56(2):1247–1252, 2023. doi:[10.1016/j.ifacol.2023.10.1747](https://doi.org/10.1016/j.ifacol.2023.10.1747).
- [12] A. d’Aspremont, D. Scieur, and A. Taylor. Acceleration methods. *Foundations and Trends® in Optimization*, 5(1–2):1–245, 2021. doi:[10.1561/24000000036](https://doi.org/10.1561/24000000036).
- [13] E. A. Feinberg and A. Shwartz, editors. *Handbook of Markov Decision Processes: Methods and Applications*, volume 40 of *International Series in Operations Research & Management Science*. Springer, Boston, MA, 2002. doi:[10.1007/978-1-4615-0805-2](https://doi.org/10.1007/978-1-4615-0805-2).
- [14] H. J. Ferreau, C. Kirches, A. Potschka, H. G. Bock, and M. Diehl. qpOASES: a parametric active-set algorithm for quadratic programming. *Mathematical Programming Computation*, 6(4):327–363, 2014. doi:[10.1007/s12532-014-0071-1](https://doi.org/10.1007/s12532-014-0071-1).
- [15] A. Ghannad, D. Orban, and M. A. Saunders. Linear systems arising in interior methods for convex optimization: a symmetric formulation with bounded condition number. *Optimization Methods and Software*, 37(4):1344–1369, 2022. doi:[10.1080/10556788.2021.1965599](https://doi.org/10.1080/10556788.2021.1965599).
- [16] P. Gill, W. Murray, and M. Wright. *Practical Optimization*. Academic Press, 1981. URL <https://books.google.de/books?id=xUzvAAAAAAAJ>.
- [17] P. E. Gill and D. P. Robinson. A primal-dual augmented Lagrangian. *Computational Optimization and Applications*, 51(1):1–25, 1 2012. doi:[10.1007/s10589-010-9339-1](https://doi.org/10.1007/s10589-010-9339-1).
- [18] P. Giselsson and S. Boyd. Linear convergence and metric selection for Douglas–Rachford splitting and ADMM. *IEEE Transactions on Automatic Control*, 62(2):532–544, 2017. doi:[10.1109/TAC.2016.2564160](https://doi.org/10.1109/TAC.2016.2564160).
- [19] B. Goujaud, C. Moucer, F. Glineur, J. M. Hendrickx, A. B. Taylor, and A. Dieuleveut. Pepit: computer-assisted worst-case analyses of first-order optimization methods in python. *Mathematical Programming Computation*, 16(3):337–367, 2024. doi:[10.1007/s12532-024-00259-7](https://doi.org/10.1007/s12532-024-00259-7).
- [20] L. Grippo, F. Lampariello, and S. Lucidi. A nonmonotone line search technique for newton’s method. *SIAM Journal on Numerical Analysis*, 23(4):707–716, 1986. doi:[10.1137/0723046](https://doi.org/10.1137/0723046).
- [21] B. Hermans, A. Themelis, and P. Patrinos. QPALM: a proximal augmented lagrangian method for nonconvex quadratic programs. *Mathematical Programming Computation*, 14(3):497–541, 2022. doi:[10.1007/s12532-022-00218-0](https://doi.org/10.1007/s12532-022-00218-0).
- [22] J. Ichnowski, P. Jain, B. Stellato, G. Banjac, M. Luo, F. Borrelli, J. E. Gonzalez, I. Stoica, and K. Goldberg. Accelerating quadratic optimization with reinforcement learning. In M. Ranzato, A. Beygelzimer, Y. Dauphin, P. Liang, and J. W. Vaughan, editors, *Advances in Neural Information Processing Systems*, volume 34, pages 21043–21055. Curran Associates, Inc., 2021. URL https://proceedings.neurips.cc/paper_files/paper/2021/file/afdec7005cc9f14302cd0474fd0f3c96-Paper.pdf.
- [23] L. P. Kaelbling, M. L. Littman, and A. R. Cassandra. Planning and acting in partially observable stochastic domains. *Artificial Intelligence*, 101(1):99–134, 1998. doi:[https://doi.org/10.1016/S0004-3702\(98\)00023-X](https://doi.org/10.1016/S0004-3702(98)00023-X).
- [24] K. Li and J. Malik. Learning to optimize. In *International Conference on Learning Representations*, 2017, 1606.01885. URL <https://openreview.net/forum?id=ry4Vrt5gl>.
- [25] E. Liang, R. Liaw, R. Nishihara, P. Moritz, R. Fox, K. Goldberg, J. E. Gonzalez, M. I. Jordan, and I. Stoica. RLlib: Abstractions for distributed reinforcement learning. In J. Dy and A. Krause, editors, *Proceedings of the 35th International Conference on Machine Learning*, volume 80 of *Proceedings of Machine Learning Research*, pages 3053–3062. PMLR, 2018. URL <https://arxiv.org/pdf/1712.09381>.
- [26] D. Liao-McPherson and I. Kolmanovsky. FBstab: A proximally stabilized semismooth algorithm for convex quadratic programming. *Automatica*, 113:108801, 2020. doi:[10.1016/j.automatica.2019.108801](https://doi.org/10.1016/j.automatica.2019.108801).
- [27] F. J. Luque. Asymptotic convergence analysis of the proximal point algorithm. *SIAM Journal on Control and Optimization*, 22(2):277–293, 1984. doi:[10.1137/0322019](https://doi.org/10.1137/0322019).
- [28] I. Maros and C. Mészáros. A repository of convex quadratic programming problems. *Optimization Methods and Software*, 11(1-4):671–681, 1999. doi:[10.1080/10556789908805768](https://doi.org/10.1080/10556789908805768).

- [29] N. Parikh and S. Boyd. Proximal algorithms. *Foundations and Trends® in Optimization*, 1(3):127–239, 2014. doi:10.1561/2400000003.
- [30] S. Pougkakiotis and J. Gondzio. An interior point-proximal method of multipliers for convex quadratic programming. *Computational Optimization and Applications*, 78(2):307–351, 2021. doi:10.1007/s10589-020-00240-9.
- [31] R. T. Rockafellar. Augmented Lagrangians and applications of the proximal point algorithm in convex programming. *Mathematics of operations research*, 1(2):97–116, 1976. doi:10.1287/moor.1.2.97.
- [32] R. T. Rockafellar. Monotone operators and the proximal point algorithm. *SIAM Journal on Control and Optimization*, 14(5):877–898, 1976. doi:10.1137/0314056.
- [33] R. Sambharya, G. Hall, B. Amos, and B. Stellato. End-to-end learning to warm-start for real-time quadratic optimization. In N. Matni, M. Morari, and G. J. Pappas, editors, *Proceedings of the 5th Annual Learning for Dynamics and Control Conference*, volume 211 of *Proceedings of Machine Learning Research*, pages 220–234. PMLR, 6 2023. URL <https://proceedings.mlr.press/v211/sambharya23a.html>.
- [34] R. Sambharya, G. Hall, B. Amos, and B. Stellato. Learning to warm-start fixed-point optimization algorithms. *Journal of Machine Learning Research*, 25(166):1–46, 2024. URL <http://jmlr.org/papers/v25/23-1174.html>.
- [35] J. Schulman, F. Wolski, P. Dhariwal, A. Radford, and O. Klimov. Proximal policy optimization algorithms, 2017, 1707.06347.
- [36] R. Schwan, Y. Jiang, D. Kuhn, and C. N. Jones. PIQP: A proximal interior-point quadratic programming solver. In *2023 62nd IEEE Conference on Decision and Control (CDC)*, pages 1088–1093, 2023. doi:10.1109/CDC49753.2023.10383915.
- [37] B. Stellato, G. Banjac, P. Goulart, A. Bemporad, and S. Boyd. OSQP: an operator splitting solver for quadratic programs. *Mathematical Programming Computation*, 12(4):637–672, 2020. doi:10.1007/s12532-020-00179-2.
- [38] R. S. Sutton and A. G. Barto. *Reinforcement Learning: An Introduction*. The MIT Press, second edition, 2018. URL <http://incompleteideas.net/book/the-book-2nd.html>.
- [39] A. Wächter and L. T. Biegler. On the implementation of an interior-point filter line-search algorithm for large-scale nonlinear programming. *Mathematical Programming*, 106(1):25–57, 3 2006. doi:10.1007/s10107-004-0559-y.
- [40] K. Wei, A. Aviles-Rivero, J. Liang, Y. Fu, H. Huang, and C.-B. Schönlieb. TFPnP: Tuning-free plug-and-play proximal algorithms with applications to inverse imaging problems. *Journal of Machine Learning Research*, 23(16):1–48, 2022. URL <http://jmlr.org/papers/v23/20-1297.html>.
- [41] Z. Wu, E. Liang, M. Luo, S. Mika, J. E. Gonzalez, and I. Stoica. RLlib flow: Distributed reinforcement learning is a dataflow problem. In *Conference on Neural Information Processing Systems (NeurIPS)*, 2021. URL <https://proceedings.neurips.cc/paper/2021/file/2bce32ed409f5ebcee2a7b417ad9beed-Paper.pdf>.